

Ballast degradation

Effect of particle size and shape using Los Angeles Abrasion test and image analysis

Guo, Yunlong; Markine, Valeri; Song, Jianing; Jing, Guoqing

DOI

[10.1016/j.conbuildmat.2018.02.170](https://doi.org/10.1016/j.conbuildmat.2018.02.170)

Publication date

2018

Document Version

Accepted author manuscript

Published in

Construction and Building Materials

Citation (APA)

Guo, Y., Markine, V., Song, J., & Jing, G. (2018). Ballast degradation: Effect of particle size and shape using Los Angeles Abrasion test and image analysis. *Construction and Building Materials*, 169, 414-424. <https://doi.org/10.1016/j.conbuildmat.2018.02.170>

Important note

To cite this publication, please use the final published version (if applicable). Please check the document version above.

Copyright

Other than for strictly personal use, it is not permitted to download, forward or distribute the text or part of it, without the consent of the author(s) and/or copyright holder(s), unless the work is under an open content license such as Creative Commons.

Takedown policy

Please contact us and provide details if you believe this document breaches copyrights. We will remove access to the work immediately and investigate your claim.

Ballast degradation: effect of particle size and shape using Los Angeles Abrasion test and image analysis

Yunlong Guo¹, Valeri Markine¹, Jianing Song², Guoqing Jing^{2*}

1. Faculty of Civil Engineering and Geosciences, Delft University of Technology, Delft, 2628CN, Netherlands

2. School of Civil Engineering, Beijing Jiaotong University, Beijing, 100044, China

yunlong.guo@tudelft.nl; V.L.Markine@tudelft.nl; 354932182@qq.com; gqjing@bjtu.edu.cn;

* Corresponding author

Abstract:

Ballast track is the most widely used track for the railway transport, and ballast bed plays a significant role to provide resistances during train operation. Generally, the ballast bed consists of crushed stones. To achieve the mitigation of ballast degradation, the first priority is to describe the degradation development and to study its effect factors.

The influence of ballast morphology (particle size and shape) on ballast degradation is examined here using the Los Angeles Abrasion (LAA¹) test in combination with 3-D image analysis. LAA tests are used to obtain the deteriorated ballast. Then, based on the 3-D images, the changes of ballast particles after the tests were analysed. To quantify the ballast degradation (abrasion and breakage), the Abrasion Depth based on the analysis of 3-D images were proposed, while ballast breakage was estimated using the broken particles ratio.

The results have shown that ballast degradation is directly related to the ballast morphology. The proposed image-based procedure can effectively be applied to assess ballast degradation. The results can be used for ballast material standardization, modelling of ballast degradation process and maintenance cycle prediction.

Key words: Ballast; Los Angeles Abrasion test; Image analysis; Ballast degradation; Ballast morphology

1 Introduction

Ballast bed used in railway track design (Figure 1) traditionally consists of crushed hard rocks with average particle size range of 20 mm–65 mm under the sleeper, with high density, toughness, hardness, and high resistance to weathering. Ballast shear strength is influenced by ballast compaction, particle state and particle size distribution, and generally fresh ballast particles contribute more to ballast resistance .

LAA test: Los Angeles Abrasion test

LAA loss: Los Angeles Abrasion loss

DEM: Discrete Element Method

FI: flakiness index

EI: elongation index

AAD: Average Abrasion Depth

MAD: Maximum Abrasion Depth

SLAV: Single LAA loss calculated with volume

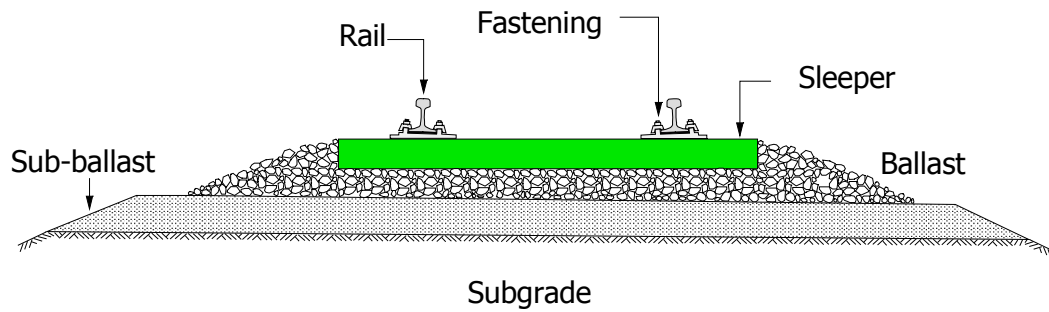


Figure 1 Traditional railway track

A main problem of the traditional railway tracks is geometry deterioration, which is mainly related to the track settlement. Most of the settlement is caused by the permanent deformation of the ballast layer [1], which results from densification or dilation, distortion, and degradation, as concluded in [2]. Because ballast undergoes gradual and continuing degradation due to the cyclic loadings and the maintenance operations, researchers keep developing methods (examples in [3-5]) to study ballast bed degradation. Nevertheless, some issues are still controversial, such as the effects of shape and size on degradation and deformation.

As the research in [2, 6], it was demonstrated that the particle's shape and roughness influences the ballast resistance and shear strength, and comparing to the rounded particles, the angular ones contribute to lower permanent deformation [7]. However, higher particle angularity is related with the increasing of breaking strain and the reduction of the ballast stiffness. Another study on particle shape shows that flaky or elongated particles at a limited percentage could increase the shear strength, and reduce the settlement for the lower rate of settlement accumulation [8]. However, it was also reported that flaky or elongated particles would lead to increased particle degradation and higher deformation [9]. Likewise, there is no general consensus on the effect of particle size [10]. It was found that particle size has little influence on shear strength in [11]. Yet, it was concluded in [12] that the shear strength increases when the particle size reduces. Conversely, the shear strength increases as the particle size increasing according to the research in [13].

It is difficult to obtain unified principles of ballast study for it is granular material. Plenty of effect factors will contribute to the final results causing no trends, if the ballast is only treated as a whole sample. For instance, when studying how the ballast size influences the shear strength, the compaction and bulk density might be the key factors [14]. However, during the adding normal stress or the shearing process, the ballast breakage will change the compaction and also the contacts. It may become a key factor, if ballast breakage is very severe [15]. For that, it needs to study from the granular level other than analysing the trends according to the test results of the whole sample. Therefore, it is significant to develop a method to estimate individual ballast particle degradation, and based on that, the effect of the factors, such as the shape, and the size, could be quantified accurately.

In order to obtain the deteriorated ballast the Los Angeles Abrasion (LAA) test was used. Generally, it is used for measuring toughness of grain materials. For this part, several laboratory tests, for instance, the Los Angeles abrasion test(LAA), mill abrasion test, Deval abrasion test, were used for the studies of ballast degradation and generation of fouled ballast [5, 16]. However, the mill abrasion test cannot simulate the impact during train passing. And the abrasion results after the micro-Deval tests did not exerts any relationship with the degradation of ballast under repeated loading [17]. Although LAA test may not fully simulate the effect of field loading conditions [18], it was found that results of LAA test are well-correlated with ballast box test results when tamping was considered in their experiments [19, 20].

During the test the material samples and a set of steel spheres are tumbled inside a closed, hollow, steel cylinder (Figure 2), which is rotated around a horizontal axis. The LAA test is an effective and simple way to obtain deteriorated ballast and the fouling, and for this purpose it was used in [21-23].

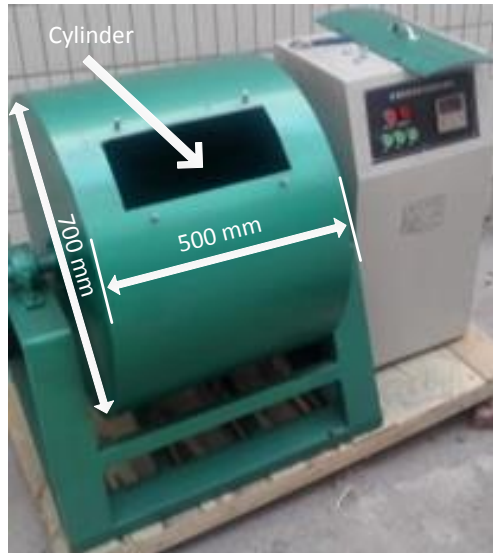


Figure 2 Los Angeles Abrasion (LAA) test machine

A comprehensive tests were performed in [17], finding that the LAA results correlated fairly well with ballast breakage of the full scale track model test. It also concluded that the LAA test can distinguish high-quality material and the poor material clearly. It was proposed in [24] that, the sieve analysis that is used in the LAA test for determining how the particles reduce in size, is not precise enough to estimate the ballast degradation, especially for the purpose of numerical simulations e.g. using Discrete Element Method (DEM).

Recently, ballast degradation was studied and determined from the digital or X-ray images system by various researchers [21, 25-27]. Detailed measurements of particle's shape and roughness using the image analysis method have been successfully used for quantifying particle morphology [28, 29]. Ballast particle abrasion and breakage by LAA tests with fouling index, and a relationship between the fouling index and the flakiness and elongation index change, sharp corner loss and surface texture reduction of the ballast particles, and the ballast shape factors evolution in different LAA test stages were studied in [21]. However, how individual ballast particles with various morphology deteriorate have not been systematically studied. Moreover, the digital or X-ray image is a cross section of an individual particle, and reflects the morphology of ballast particles roughly. As proposed in [27], only when the number of cross-sections is sufficiently large, the morphology of ballast particles can be more accurately accessed, however, it is quite time consuming.

As a consequence, this paper describes a study to measure and evaluate how an individual particle morphology (size and shape) changes during degradation. It is studied with LAA tests, as well as 3-D image analysis. Based on the 3-D images, quantifications of individual particle changes in detailed parameters are proposed and studied. 3-D image analysis is an ideal and accurate tool for quantifying particle size and shape properties in a rapid, reliable and automated fashion when compared to traditional manual methods, confirmed in [25, 26, 30-32]. Ballast images from laser scanning are utilized to record initial ballast morphology, afterward the LAA test was conducted to obtain the deteriorated ballast particles. Comparing the images before and after LAA tests can reveal the changes on form, surface texture and sharp corner of ballast particles [33], as well as ballast breakage, and then demonstrate the main form of ballast degradation. In addition, based on the image analysis method, the effect factors were studied, such as particle shape and size. Using image analysis to study ballast degradation could estimate ballast bed condition, so that can provide guidance on maintenance. Moreover, the 3-D images can be applied in the DEM models as the particle templates to simulate the irregular shape and sharp corners in the future research.

2 Analysis of ballast degradation

In this section, the detailed test procedure to analyse ballast degradation is introduced, including sample processing, the LAA test and laser scanning. In addition, the methods applied to estimate ballast degradation are described.

2.1 Test planning

With the aim of studying the ballast degradation, the test procedure is designed, as shown in Figure 3. Also, the goal of the test was to verify the assumptions that the ballast degradation mainly results from sharp corner loss, and that the flaky or elongated particles are more prone to break.

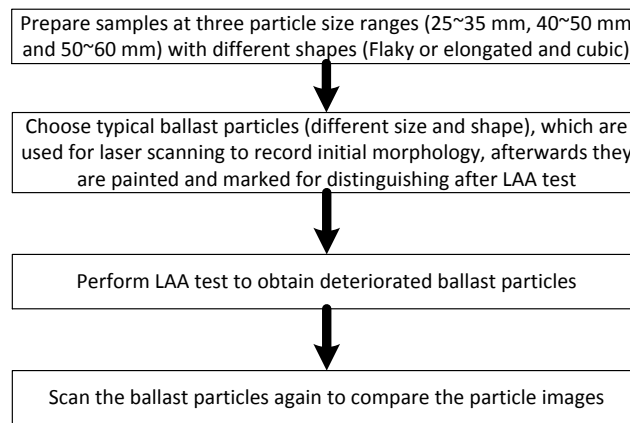


Figure 3 Test flow chart

2.1.1 Samples processing

In order to study effect factors of ballast degradation, the ballast particles were categorized by their shapes as flaky or elongated and cubic, according to the flakiness and elongation index suggested in [34-36]. By their size, three particle size ranges are categorized, namely 25~35 mm, 40~50 mm and 50~60 mm.

The flakiness and elongation index is quantified with the lengths of the three representative axes: the longest axis with the length L , the medium axis with the length I and the shortest axis with the length S . The medium axis length I is treated as the sieve size, which was proposed in [21, 25, 35, 37, 38]. After measuring the three axes of each particle, the flakiness index (FI) and elongation index (EI) for each particle are obtained as follows:

$$\text{Equation 1 } FI = S / I$$

$$\text{Equation 2 } EI = I / L$$

As shown in Figure 4, the ballast particles with FI smaller than 0.6 or with EI above 1.8 as the flaky or elongated ballast particles, according to [36]. Ballast particles that are neither elongated nor flaky are considered as the cubic ones.



Figure 4 Flaky (left) and elongated (right) ballast particles in particle size range of 25~35 mm

The ballast material used in the tests was crushed granite as shown in Figure 5. The ballast particles were washed with fresh water, and then dried in open air for 3 days. After that the particles were selected and measured to calculate the flakiness and elongation index. The ballast particles were sieved into 3 groups at the size range of 25~35 mm, 40~50 mm and 50~60 mm respectively, and each group weighs 5 kg, including cubic, flaky or elongated particles.

The scanned (will be explained in the next Section 2.1.2), flaky or elongated and cubic particles were painted into three different colors and each particle is marked with a certain number, for being distinguished after the LAA test. To be more specific, the cubic particles are red, the flaky or elongated ones are black, as shown in Figure 5b.



Figure 5 (a) Sample preparation; (b) Sample particle size ranges: 50~60 mm (left), 40~50 mm (middle), 25~35 mm (right)

2.1.2 Scanning ballast particles

In order to study how the shape of ballast particles influences ballast degradation, some of the particles were scanned for subsequent analysis using the laser scanner. The scanned ballast particles, chosen from the 3 different size ranges, contain flaky or elongated and cubic ones. In order to be distinguished from the ballast particles that were not scanned, they were painted using blue color (Figure 5b). The Capture Mini Scanner used here (Figure 6) has been optimized to meet the needs of product development and engineering professionals to obtain the most effective and reliable way to acquire 3-

D measurements of physical objects. The scanner parameters are listed in Table 1.



Figure 6 Capture Mini Scanner

Table 1 Capture Mini Scanner properties

Property	Capture Mini
Weight	1.04 kg
Dimensions (L × W × H)	155 × 109 × 49 mm
Data Capture Rate	985,000 points/scan (0.3 sec per scan)
Resolution	0.080 mm at 157 mm 0.100 mm at 227 mm
Accuracy	0.034 mm
Stand-off Distance	157 mm
Depth of Field	70 mm
Field of View	87 × 68 mm (near) 88 × 87 mm (far)

The scanning process is as follow: firstly, a ballast particle is placed on a black turntable, which can spin during scanning process to get images of every particle side; secondly, the laser light reflected from particle surface is captured by coupled device camera; thirdly, about 500,000 vertices are transmitted to the computer, and three consequent images are used to form one triangular plane. Finally, all small triangular planes constitute the 3-D ballast particle image (Figure 7).

After getting the 3-D images, the next step is to reduce the noise and cover small holes resulting from data deficiency. The areas of all the triangular planes are summed up, to calculate the surface area of the 3-D particle, whereas the volume is obtained by summing up all the tetrahedral meshes. The method for calculation of volume and surface area is described in [37].

As suggested in [39], the highest resolution of 0.080 mm, is used during the scanning process for better analysis of ballast surface texture change [33]. Three images of one ballast particle with various resolutions are shown in Figure 7. From this figure it can be seen that the highest resolution can better present the surface texture.

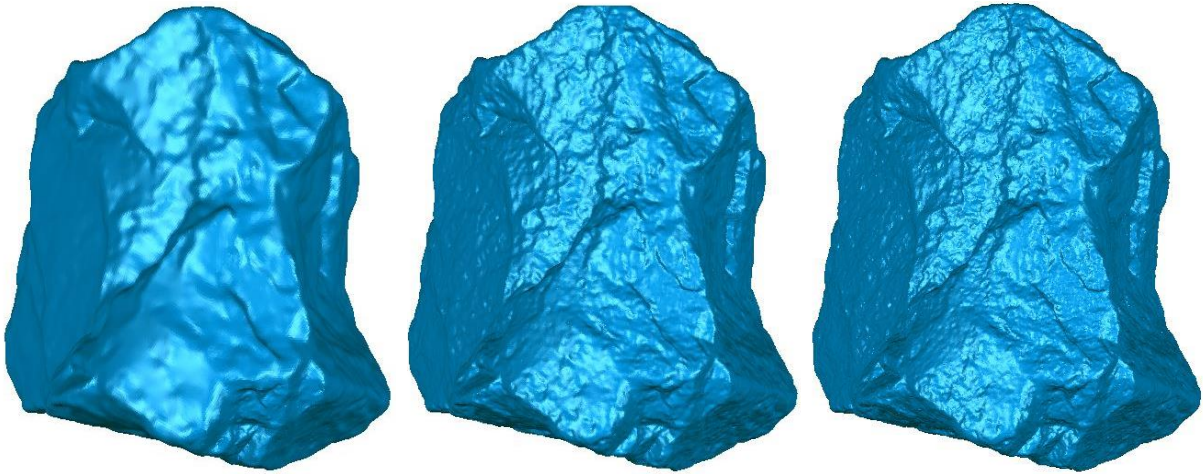


Figure 7 Images of one ballast particle with 3 resolutions: low (left); medium (middle); high (right)

2.1.3 LAA test

The dynamic behavior and deformation of rock particles subject to train loading can be generally studied by the cyclic triaxial and resonant cylinder tests, and parameters from these tests are commonly used as the indices of ballast degradation [2, 40, 41]. A common test for particle abrasion and fragmentation is the LAA test. It mainly causes fragmentation due to impact from steel balls, and more rounding shape of particles result from abrasion, as proposed in [17].

Generally, the LAA tests are used to analyse durability and strength properties of granular materials. For instance, in [42] the correlation between the material loss (also called LAA loss that will be described in Section 2.2.1) and some physical properties, including bulk density, hardness, and point load index. In [43], 35 different rock types were utilized to study the correlation between the LAA loss and uniaxial compressive. These studies focused on the correlation between the LAA loss and mechanical properties. LAA tests can also be used to obtain deteriorated ballast, confirmed in [16, 22, 23, 44]. With this method, the deteriorated ballast particles are produced.

The LAA machine has revolving speed at 31~33 r/min, and is filled with samples and steel balls. According to [36], the drum was set to rotate 1,000 turns. However, it was halted every 250 turns during the test, in order to make sure the painted particles were still with colors. After conducting the test, small particles with diameter below 1.7mm were sieved out.

After that, the particles were separated into 3 groups according to the remained color (red, black and blue) and marked number, and all particles in each size range were washed, measured and weighed.

2.1.4 Laser Scanning after LAA test

After the LAA test, the ballast particles with blue color were scanned again, as shown in Figure 8. Afterwards, the particle changes during LAA test can be studied. The ballast particles before and after the LAA test could be matched by the shape, size and marked numbers.

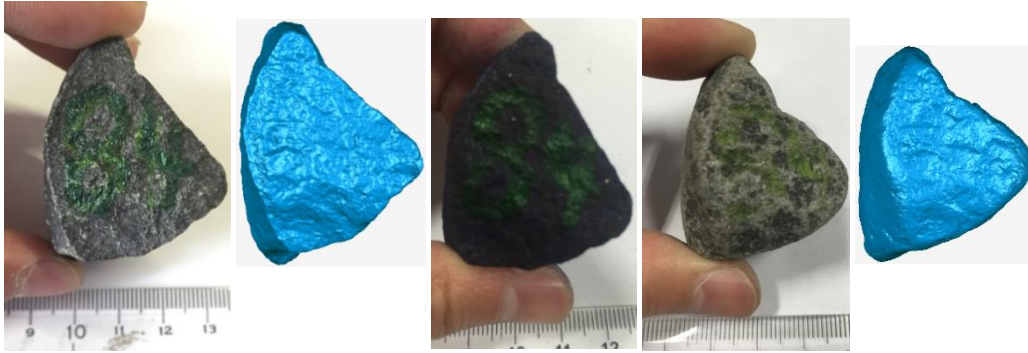


Figure 8 Scanned ballast particle and image; From left to right: initial ballast particle, initial image, painted particle, particle after test, particle image after test

2.2 Degradation estimation

In Figure 9, the main properties of the ballast particle shape are shown. They are form, sharp corner and surface texture, and their definitions are explained in [33]. They are used to characterise the shape, because each of them is essentially independent properties of the shape, and can be varied without affecting the other two properties, as proposed in [35]. More importantly, they are among the properties of ballast particles that have great influence on the performance of ballast bed (durability, shear strength and stiffness), by influencing mutual contacts [10, 45]. Another significant factor affecting the performance of ballast layer is the ballast breakage. Because it has correlation with the strength, modulus, bulk density and internal friction [12, 15]. Consequently, an extensive study is necessary to clarify the ballast degradation mechanism, including the sharp corner loss, breakage, and surface texture reduction, applicable to railway ballast.

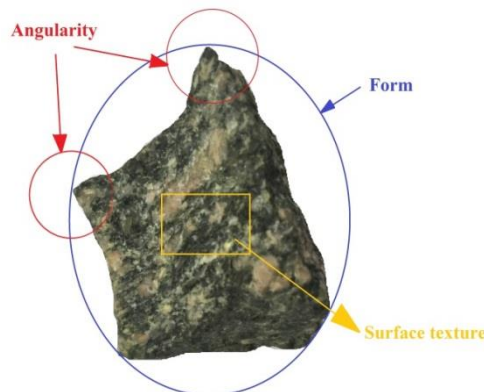


Figure 9 Shape properties of ballast particle

However, most of research studies focused on quantifying ballast shape properties. A limited number of studies were performed on investigating the changing of the shape properties with 2-D images analysis [23]. To date, no studies has yet reported to use 3-D images for analyzing the shape property changing of individual ballast particles. More importantly, to study the ballast breakage, various indices were proposed, such as B_g , B_r , BBI , B . Their methods are to measure the percentage of some certain sieve sizes, or to estimate the change of Particle Size Distribution (PSD) [15, 41, 46, 47]. However, that costs large amount of time, and also the results are not accurate for they are based on sieving, which always provides fluctuating results due to personal equation. Therefore, new methods are proposed as follows to study the ballast degradation.

Based on the 3D images of ballast particles, ballast degradation was estimated using the following parameters, and their definitions will be explained in the following sub-sections:

1. LAA loss (%) - the overall sample degradation estimation;
2. Broken number rate – ballast breakage

3. Image analysis

- a. Average Abrasion Depth – estimating individual ballast particle degradation
- b. 3D True Sphericity [48] – estimating form change (particles become more rounded)
- c. Maximum Abrasion Depth - estimating sharp corner change (sharp corner loss)
- d. Abrasion Depth – estimating roughness change (surface texture reduction)

2.2.1 LAA loss

The LAA loss (%) is a vital parameter characterising abrasion resistance of grain materials, as described in [42]. It is defined as the weight loss rate:

$$\text{Equation 3 } LA = (M_1 - M_2) / M_1$$

In the Equation 3, M_1 is the initial weight of tested material, and the M_2 is the weight of tested material after the LAA test.

2.2.2 Broken particles ratio

To obtain the correlation between the shape/size and ballast breakage, for the scanned particles, the broken ballast particles are counted. To be more specific, after picking out the scanned particles according to color, they were compared with their initial images. However, some of the particles cannot match any of the initial images, because they were broken during the test (Figure 10). Ballast breakage can be assessed by the broken particles ratio defined as the ratio between the number of the broken particles and the initial number of the particles.



Figure 10 Example of broken ballast particle that cannot match any of the initial images

2.2.3 3D True Sphericity

During the LAA test, the ballast particles deteriorate with the form changing to more rounded. In order to quantify it, the “3D true Sphericity”, proposed in [48], was used in this study. Obtaining this parameter includes three steps: the first step is to measure the volume of a ballast particle (V_0), which is used to calculate the radius r of the sphere with equivalent volume from

$$\text{Equation 4 } V_0 = \frac{4}{3} \pi r^3$$

Then the radius r is used to calculate the surface area of the sphere, S :

$$\text{Equation 5 } S = 4\pi r^2$$

Finally, the “3D True Sphericity”, ψ , is calculated as the ratio between the surface area of the sphere,

S , and the surface area of ballast particle, S_0 .

$$\text{Equation 6 } \psi = S / S_0$$

2.2.4 Abrasion Depth

The Abrasion Depth is calculated by comparing the two images to obtain the difference values, as shown in Figure 11.

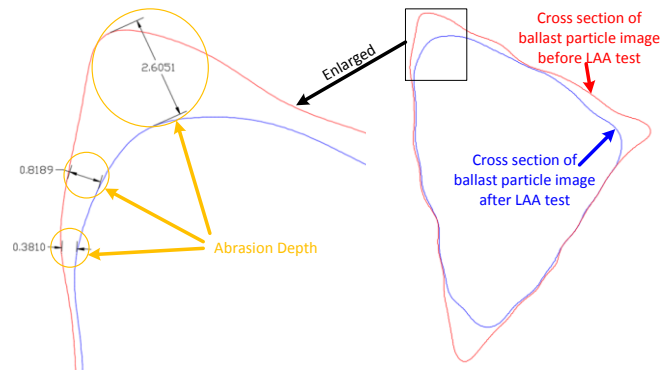


Figure 11 Explanation of Abrasion Depth calculation

As shown in Figure 12, the Abrasion Depth result shows the degree of abrasion in different zones, including sharp corners, edges, and flat surfaces.

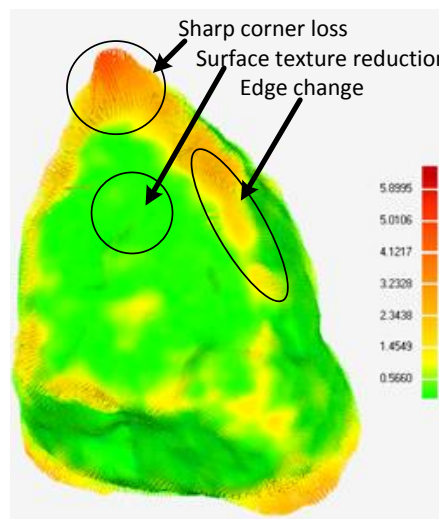


Figure 12 Abrasion Depth (in mm) of one ballast particle obtained from 3-D image analysis

Based on the Abrasion Depth, an alternative method, the Average Abrasion Depth (AAD), is proposed to evaluate individual ballast degradation. The AAD is calculated by averaging the summation of all the Abrasion Depth of one ballast particle. This parameter can be utilized to present the deterioration degree of an individual ballast particle, which will be verified in the Section 2.2.5.

Another parameter, the Maximum Abrasion Depth (MAD), is used to estimate the sharp corner loss of ballast particles. It is also based on the Abrasion Depth. As shown in Figure 12, the maximum value of the Abrasion Depth is at the sharp corner that is around 5.90 mm (dark red color). It is defined as the MAD .

As shown in Figure 12, it can be seen that the green part corresponds to the Abrasion Depth in the range of 0.0~0.57 mm. It generally occurs at the flat surface, which is treated as the surface texture reduction.

2.2.5 LAA loss of single particles

The LAA loss is for the whole sample (overall ballast particles) and is not suitable for degradation analysis of individual ballast particle. Therefore, the Single LAA loss parameter is introduced. It is the material loss of every individual ballast particles after the LAA test. It can be calculated on the basis of mass or volume of a ballast particle (Equation 7 and Equation 8). In the equations: M_1 is the initial mass, V_1 is the initial volume; The M_2 and V_2 are mass and volume after the LAA test respectively.

$$\text{Equation 7 } SLAM = (M_1 - M_2) / M_1$$

$$\text{Equation 8 } SLAV = (V_1 - V_2) / V_1$$

Volume is also available from image analysis, and it is more accurate than mass measurement, confirmed in [24, 49]. The Single LAA loss calculated with volume ($SLAV$) is used to verify if the AAD can be utilized to estimate ballast degradation. The correlation between the AAD value and $SLAV$ is shown in Figure 13. It can be seen there is a linear relation between the AAD and $SLAV$.

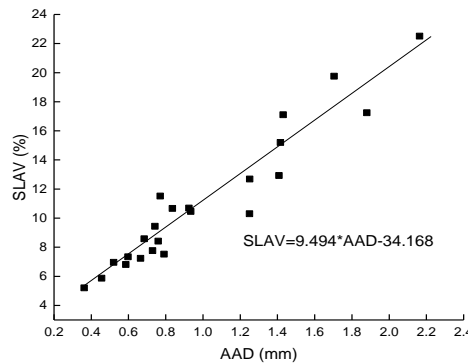


Figure 13 Average Abrasion Depth versus $SLAV$ (Single LAA loss calculated by volume)

3 Results and discussion

In this section, all the results on degradation estimation are listed in detail. The LAA loss of two shape groups (cubic and flaky or elongated) are compared. After that, the scanned ballast particles (Defined in Section 2.1.2) are analysed, as follow.

Firstly, the broken condition is analysed, showing how shape and size influences the ballast particle breakage.

Additionally, comparing the value change of the “3D true Sphericity” in different size range helps obtain how particle size influences form change of ballast particle (more rounded).

Finally, the MAD and AAD are utilized for the analysis of particle sharp corner loss and individual degradation respectively.

3.1 LAA loss results

Table 2 shows the LAA loss results of three particle size ranges according to Equation 3. The results of flaky or elongated as well as the cubic particles are compared. From the results, it can be observed that the LAA loss of flaky or elongated particles is higher than of the cubic particles, which predicts the flaky or elongated ballast particles deteriorate more seriously.

Table 2 LAA loss of three particle size groups; the flaky or elongated and cubic LAA loss

Particle size	50~60 mm	40~50 mm	25~35 mm
Flaky or elongated	15.10	19.28	16.17
Cubic	4.15	5.37	11.67

3.2 Breakage analysis results

By counting the broken particles ratio (defined in Section 2.2.2) of scanned particles, the results are listed in Table 3. From the table, it can be concluded that flaky or elongated particles are more prone to crack than the cubic particles. In addition, bigger ballast particles crack more easily. The explanations are listed below:

1. The broken particles ratio of cubic particles are 0% (25~35 mm), 25% (40~50 mm) and 50% (50~60 mm), which are lower than the flaky or elongated particles at 41.7% (25~35 mm), 58.3% (40~50 mm) and 77.8% (50~60 mm).
2. When it comes to the particle size, the total broken number rate of three groups are 31.3% (25~35 mm), 50% (40~50 mm) and 69.2% (50~60 mm) respectively, from which it can be concluded that the bigger particles are more prone to fracture.

Table 3 Number and ratio of broken ballast particles at three particle size ranges

Particle size(mm)	Total broken rate(%)	Shape	Scanned particle number	Broken particle number	Broken particles ratio(%)
25~35	31.30	cubic	4	0	0.00
		flaky or elongated	12	5	41.70
40~50	50.00	cubic	4	1	25.00
		flaky or elongated	12	7	58.30
50~60	69.20	cubic	4	2	50.00
		flaky or elongated	9	7	77.80

3.3 3D true Sphericity analysis results

Based on the data (volume and surface area) in Table A.1 at appendix, the data in Table 4 can be obtained. Table 4 presents the average “3D true Sphericity” value before and after the LAA test at two particle size ranges (25~35 mm and 40~50 mm). The particle size range 50~60 mm was not used for analysis, because it only has 4 unbroken particles left after the LAA test, which influences a lot on the “3D true Sphericity” value.

According to the data in Table A.1, the volume and surface area of every particles decrease after the LAA test, while, the “3D true Sphericity” values increase. It was proposed in [48] that the “3D true Sphericity” value is in the range of 0.000~1.000, and the value is closer to 1.000 for the more rounded particles. The increased “3D true Sphericity” value indicates that the LAA test can cause significant changes of the particle form, which means ballast particles became smoother and more rounded. Rounded particles will lead to less stable particle interlocking than the fresh ballast.

Table 4 Average “3D true Sphericity” value before and after LAA test

Particle size	Average 3D true Sphericity before test	Average 3D true Sphericity after test	Value change rate (%)
25~35 mm	0.747	0.806	7.89
40~50 mm	0.728	0.806	10.63

From Table 4, it can be seen that the value change rate of particle size range at 40~50 mm is 10.63%, which is bigger than 7.89% (value change rate of particle size range at 25~35 mm). It indicates that

particle size influences ballast degradation during the LAA test, which means bigger particles are more prone to become rounded.

3.4 MAD and AAD analysis results

From the Figure 14, it can be seen that the most serious abrasion zone occurs at the sharp corner, so the *MAD* value can be used to quantify sharp corner loss, as described in Section 2.2.4.

It can also be observed that the serious abrasion zones mostly occur at sharp corners and edges, and that less Abrasion Depth appears at the flat surface with the value within 1.00 mm. The image analysis results are consistent with cyclic triaxial tests in [41], identifying that most ballast degradation is primarily the consequence of sharp corner loss.

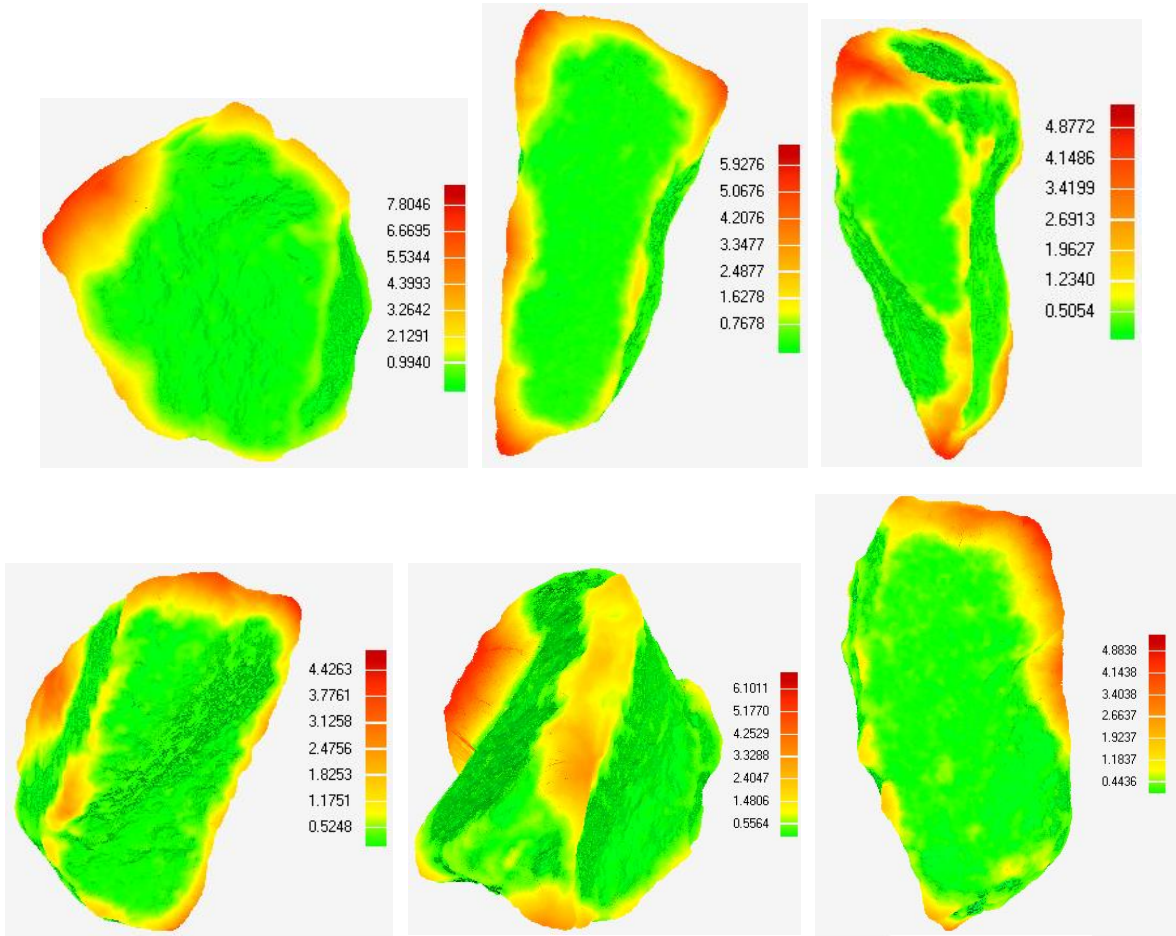


Figure 14 Abrasion Depth (in mm) of ballast particles

Figure 15 shows the average *MAD* and average *AAD* value at two size ranges (25~35 mm and 40~50 mm). The two size ranges (25~35 mm and 40~50 mm) are used for analysis, because the particle size range 50~60 mm has only 4 unbroken particles left after the LAA test, which influences a lot on the average value.

As shown in Figure 15, the flaky or elongated particles have higher average *AAD* and average *MAD* than the cubic particles, indicating that flaky or elongated particles deteriorate more seriously and lost their sharp corners more easily.

In addition, the particle size range 40~50 mm shows higher average *AAD* and average *MAD* than the size range 25~35 mm, proving that bigger ballast particles deteriorate more seriously and lose sharp corners more easily.

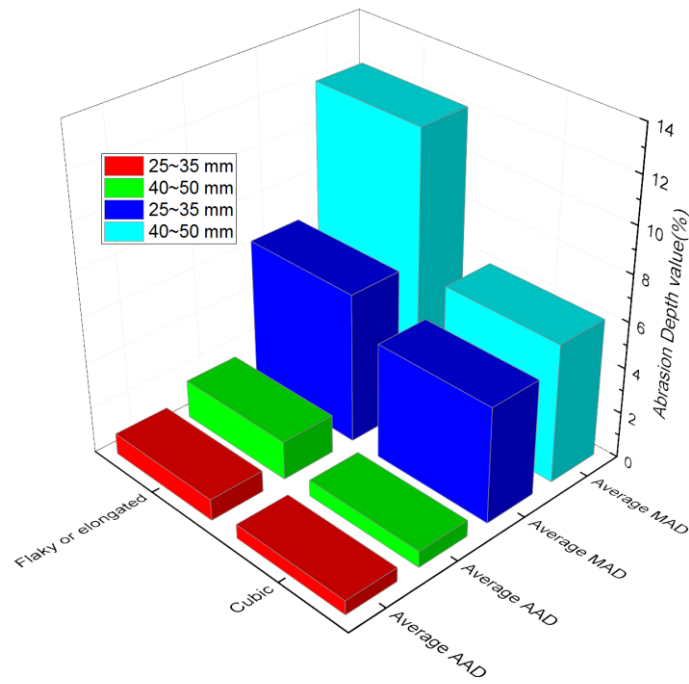


Figure 15 Test results: Average MAD and average AAD value for different particle size and shape

4 Conclusions and perspective

Proposing a new method (Abrasion Depth) to quantify ballast degradation, obtaining the ballast degradation mechanism, as well as obtaining the effect factors of ballast degradation are the main purposes of this study. To achieve that, the LAA test was used to artificially obtain deteriorated ballast particles. Afterwards, the image analysis method was used to assess ballast degradation. The form change, breakage, sharp corner loss and surface texture reduction of the ballast were quantified by analysing the *MAD*, *AAD*, LAA loss and the “3D true Sphericity” parameters.

Conclusions on methodology:

- The method employed, consisting of the LAA tests and the 3-D image analysis, allows the quantified assessment of the ballast degradation, especially in cases of abrasion degradation of individual ballast particle.

Based on the results of the analysis, the following conclusions are drawn:

- The ballast morphology (particle size and shape) influences the ballast degradation:
 - a. Comparing to the cubic ballast particles, the flaky or elongated ballast particles loss more volume and loss sharp corners more easily.
 - b. The flaky or elongated ballast particles are more prone to crack than the cubic particles.

Since both contribute to ballast pollution and degradation of the ballast bed, the presence of flaky and elongated is not desirable.

- The main form of ballast degradation is sharp corner loss, so the ballast particles with corners which are not very sharp should be used more in ballast bed.
- As expected, the volume and surface area of every particle decrease during the LAA tests. The bigger ballast particles become more rounded and are more prone to crack. Since rounded

particle and particle breakage are not desirable in ballast bed, the proper particle size should be used in ballast bed.

Perspective:

- The results obtained here together with the 3-D image analysis will be used in the detailed numerical simulations using DEM to analyse the degradation mechanism of ballast.
- In addition, the method based on the 3-D image analysis to quantify ballast degradation could be used to assess the ballast bed condition and to predict the maintenance cycle.

Acknowledgments

The paper was supported by the Natural Science Foundation of China (Grant No.51578051) and China Scholarship Council.

Reference

- [1] D. Li, J. Hyslip, T. Sussmann, S. Chrismer, *Railway geotechnics*, CRC Press 2002.
- [2] Q.D. Sun, B. Indraratna, S. Nimbalkar, Deformation and degradation mechanisms of railway ballast under high frequency cyclic loading, *Journal of Geotechnical and Geoenvironmental Engineering* 142(1) (2015) 04015056.
- [3] N.T. Ngo, B. Indraratna, Improved performance of rail track substructure using synthetic inclusions: experimental and numerical investigations, *International Journal of Geosynthetics and Ground Engineering* 2(3) (2016) 24.
- [4] E. Kabo, A numerical study of the lateral ballast resistance in railway tracks, *Proceedings of the Institution of Mechanical Engineers, Part F: Journal of Rail and Rapid Transit* 220(4) (2006) 425-433.
- [5] H. Huang, E. Tutumluer, W. Dombrow, Laboratory characterization of fouled railroad ballast behavior, *Transportation Research Record: Journal of the Transportation Research Board* (2117) (2009) 93-101.
- [6] H. Huang, E. Tutumluer, Discrete Element Modeling for fouled railroad ballast, *Construction and Building Materials* 25(8) (2011) 3306-3312.
- [7] R. Knutson, M. Thompson, T. Mullin, S. Tayabji, *BALLAST AND FOUNDATION MATERIALS RESEARCH PROGRAM. PHASE IV. MATERIALS EVALUATION STUDY*, 1977.
- [8] T. Siller, Properties of railroad ballast and subballast for track performance prediction, Master's project report. Concrete Tie Correlation Study, Department of Civil Engineering, University of Massachusetts, Amherst (1980).
- [9] Y. Gur, E. Shklarsky, M. Livneh, Effect of coarse-fraction flakiness on the strength of graded materials, *Asian Conf Soil Mech & Fdn E Proc/Is/*, 1967.
- [10] D. Ionescu, Evaluation of the engineering behaviour of railway ballast, (2004).
- [11] W. Holtz, H.J. Gibbs, Triaxial shear tests on pervious gravelly soils, *Journal of the Soil Mechanics and Foundations Division* 82(1) (1956) 1-22.
- [12] N.D. Marachi, C.K. Chan, H.B. Seed, Evaluation of properties of rockfill materials, *Journal of Soil Mechanics & Foundations Div* 97(SM1) (1900).
- [13] C. Dunn, P. Bora, Shear strength of untreated road base aggregates measured by variable lateral pressure triaxial cell, *Journal of Materials* 7(2) (1972).
- [14] Z. Wang, G. Jing, Q. Yu, H. Yin, Analysis of ballast direct shear tests by discrete element method under different normal stress, *Measurement* 63 (2015) 17-24.

- [15] R.J. Marsal, Mechanical properties of rockfill, Publication of: Wiley (John) and Sons, Incorporated (1973).
- [16] Y. Qian, H. Boler, M. Moaveni, E. Tutumluer, Y. Hashash, J. Ghaboussi, Characterizing Ballast Degradation Through Los Angeles Abrasion Test and Image Analysis, Transportation Research Record: Journal of the Transportation Research Board 2448 (2014) 142-151.
- [17] R. Nålund, Railway ballast characteristics, selection criterion and performance, Department of Civil and Transport Engineering, Norwegian University of Science and Technology, Trondheim (2014).
- [18] M. Moaveni, Y. Qian, I.I.A. Qamhia, E. Tutumluer, C. Basye, D. Li, Morphological Characterization of Railroad Ballast Degradation Trends in the Field and Laboratory, Transportation Research Record: Journal of the Transportation Research Board 2545 (2016) 89-99.
- [19] W.L. Lim, Mechanics of railway ballast behaviour, University of Nottingham, 2004.
- [20] G.R. McDowell, W.L. Lim, A.C. Collop, R. Armitage, N.H. Thom, Laboratory simulation of train loading and tamping on ballast, Proceedings of the Institution of Civil Engineers-Transport, Thomas Telford Ltd, 2005, pp. 89-95.
- [21] Y. Qian, H. Boler, M. Moaveni, E. Tutumluer, Y. Hashash, J. Ghaboussi, Characterizing ballast degradation through Los Angeles abrasion test and image analysis, Transportation Research Record: Journal of the Transportation Research Board (2448) (2014) 142-151.
- [22] J. Fernlund, 3-D image analysis size and shape method applied to the evaluation of the Los Angeles test, Engineering geology 77(1) (2005) 57-67.
- [23] Y. Qian, H. Boler, M. Moaveni, E. Tutumluer, Y.M. Hashash, J. Ghaboussi, Degradation-Related Changes in Ballast Gradation and Aggregate Particle Morphology, Journal of Geotechnical and Geoenvironmental Engineering 143(8) (2017) 04017032.
- [24] J.K. Anochie-Boateng, J.J. Komba, G.M. Mvelase, Three-dimensional laser scanning technique to quantify aggregate and ballast shape properties, Construction and building materials 43 (2013) 389-398.
- [25] L. Le Pen, W. Powrie, A. Zervos, S. Ahmed, S. Aingaran, Dependence of shape on particle size for a crushed rock railway ballast, Granular Matter 15(6) (2013) 849-861.
- [26] C. Rao, E. Tutumluer, I.T. Kim, Quantification of coarse aggregate angularity based on image analysis, Transportation Research Record: Journal of the Transportation Research Board (1787) (2002) 117-124.
- [27] L. Wang, X. Wang, L. Mohammad, C. Abadie, Unified method to quantify aggregate shape angularity and texture using Fourier analysis, Journal of Materials in Civil Engineering 17(5) (2005) 498-504.
- [28] F. Okonta, Relationships between abrasion index and shape properties of progressively abraded dolerite railway ballasts, Rock mechanics and rock engineering 47(4) (2014) 1335-1344.
- [29] F. Okonta, Effect of grading category on the roundness of degraded and abraded railway quartzites, Engineering Geology 193 (2015) 231-242.
- [30] C. Mora, A. Kwan, Sphericity, shape factor, and convexity measurement of coarse aggregate for concrete using digital image processing, Cement and concrete research 30(3) (2000) 351-358.
- [31] C. Rao, T. Pan, E. Tutumluer, Determination of coarse aggregate surface texture using image analysis, 16th ASCE Engineering Mechanics Conference, University of Washington, Seattle, 2003.
- [32] G.P. Raymond, V.A. Dyaljee, Railroad ballast load ranking classification, Journal of Geotechnical and Geoenvironmental Engineering 105(10) (1979).
- [33] J. Anochie-Boateng, J. Komba, G. Mvelase, Advanced and automated laser-based technique to evaluate aggregates, (2011).
- [34] T. Zingg, Beitrag zur schotteranalyse, 1935.
- [35] P. Barrett, The shape of rock particles, a critical review, Sedimentology 27(3) (1980) 291-303.
- [36] T.P.M.o. Railways, Railway Ballast, TB/T2140-2008, China Railway Publishing House, Beijing, 2008.
- [37] J. Fernlund, Image analysis method for determining 3-D shape of coarse aggregate, Cement and Concrete Research 35(8) (2005) 1629-1637.

- [38] Y. Sun, B. Indraratna, S. Nimbalkar Dr, Three-dimensional characterisation of particle size and shape for ballast, (2014).
- [39] S.B. Sholts, S.K. Wärmländer, L.M. Flores, K.W. Miller, P.L. Walker, Variation in the measurement of cranial volume and surface area using 3D laser scanning technology, *Journal of forensic sciences* 55(4) (2010) 871-876.
- [40] R. Noålsund, E. Tutumluer, I. Horvli, Degradation of Railway Ballast Through Large Scale Triaxial and Full Scale Rail Track Model Tests: Comparison with Mechanical Laboratory Tests, *Proc., 10th International Conference on Bearing Capacity of Roads, Railways and Airfields*, pp. 25-27.
- [41] B. Indraratna, J. Lackenby, D. Christie, Effect of confining pressure on the degradation of ballast under cyclic loading, (2005).
- [42] I. Ugur, S. Demirdag, H. Yavuz, Effect of rock properties on the Los Angeles abrasion and impact test characteristics of the aggregates, *Materials characterization* 61(1) (2010) 90-96.
- [43] S. Kahraman, M. Fener, Predicting the Los Angeles abrasion loss of rock aggregates from the uniaxial compressive strength, *Materials Letters* 61(26) (2007) 4861-4865.
- [44] P. Tolppanen, 3-D Characterization and Degradation Analysis of Rock Aggregates, *Institutionen för anläggning och miljö*, 2001.
- [45] H. Boler, Y. Qian, E. Tutumluer, Influence of Size and Shape Properties of Railroad Ballast on Aggregate Packing, *Transportation Research Record: Journal of the Transportation Research Board* 2448 (2014) 94-104.
- [46] I. Einav, Breakage mechanics—Part I: Theory, *Journal of the Mechanics and Physics of Solids* 55(6) (2007) 1274-1297.
- [47] B.O. Hardin, Crushing of soil particles, *Journal of Geotechnical Engineering* 111(10) (1985) 1177-1192.
- [48] H. Wadell, Volume, shape, and roundness of quartz particles, *The Journal of Geology* 43(3) (1935) 250-280.
- [49] Y. Sun, B. Indraratna, S. Nimbalkar, Three-dimensional characterisation of particle size and shape for ballast, *Géotechnique Letters* 4(3) (2014) 197-202.

Appendix

Table A.1 Shape, condition after test, AAD, MAD, SLAM and SLAV of the scanned particles

Particle size: 25~35 mm														
Marked number	Shape	Condition after test	Initial weight (g)	Initial volume (mm ³)	Initial surface area (mm ²)	Initial 3D True Sphericity	Weight after test (g)	Volume after test (mm ³)	surface area after test (mm ²)	3D True Sphericity after test	SLAM (%)	SLAV (%)	AAD (mm)	MAD (mm)
2	elongated	broken	38	13260.21	3922.41	0.691	-	-	-	-	-	-	-	-
4	elongated	unbroken	70	24661.63	5525.73	0.741	65	22944.42	4934.10	0.791	7.14	6.96	0.52	4.88
13	elongated	broken	77	26882.24	6038.07	0.719	-	-			-	-	-	-
49	cubic	unbroken	44	15938.72	3961.24	0.773	39	14102.81	3517.96	0.802	11.36	11.52	0.77	6.10
50	elongated	unbroken	63	22067.62	5230.34	0.727	57	20175.21	4596.38	0.780	9.52	8.58	0.68	4.43
52	elongated	unbroken	83	29006.67	6045.01	0.755	77	26907.42	5360.34	0.810	7.23	7.24	0.67	4.88
54	elongated	unbroken	64	22639.56	5429.95	0.713	57	20220.98	4572.14	0.785	10.94	10.68	0.92	5.93
56	flaky	broken	52	29006.67	6045.01	0.755	-	-	-	-	-	-	-	-
65	elongated	broken	81	28163.33	6658.16	0.672	-	-	-	-	-	-	-	-
67	flaky	broken	26	8881.64	3063.06	0.677	-	-	-	-	-	-	-	-
69	flaky	unbroken	34	12113.18	3531.29	0.722	30	10271.73	2825.09	0.809	11.76	15.20	1.42	7.80
84	cubic	unbroken	47	16691.34	4026.51	0.784	43	15115.91	3491.40	0.847	8.51	9.44	0.74	4.97
95	flaky	unbroken	35	12523.22	3554.92	0.734	30	10380.76	2826.39	0.814	14.29	17.11	1.43	12.61
96	flaky	unbroken	41	14063.60	3796.77	0.742	35	12563.19	3281.91	0.796	14.63	10.67	0.84	5.19
100	cubic	unbroken	36	12701.29	3556.74	0.740	34	11768.93	3115.48	0.803	5.56	7.34	0.60	4.62

101	cubic	unbroken	43	15457.93	3795.02	0.791	40	14654.11	3471.33	0.834	6.98	5.20	0.36	4.53
Particle size: 40~50 mm														
Marked number	Shape	Condition after test	Initial weight (g)	Initial volume (mm ³)	Initial surface area (mm ²)	Initial 3D True Sphericity	Weight after test (g)	Volume after test (mm ³)	surface area after test (mm ²)	3D True Sphericity after test	SLAM (%)	SLAV (%)	AAD (mm)	MAD (mm)
2	elongated	unbroken	172	60142.38	10397.04	0.714	150	52367.88	8670.56	0.781	12.79	12.93	1.41	8.60
3	cubic	unbroken	75	26470.34	5313.76	0.808	71	24917.33	4863.00	0.848	5.33	5.87	0.46	5.23
5	flaky	broken	57	20032.02	5009.33	0.712	-	-	-	-	-	-	-	-
6	flaky	unbroken	62	21638.11	5436.82	0.691	47	16767.06	4076.96	0.777	24.19	22.51	2.16	12.75
7	elongated	broken	108	37872.39	8129.07	0.671	-	-	-	-	-	-	-	-
8	flaky	unbroken	70	24583.02	5999.08	0.682	55	19727.41	4511.04	0.783	21.43	19.75	1.70	11.39
10	cubic	unbroken	108	37768.54	7074.91	0.769	97	33816.26	5985.98	0.845	10.19	10.46	0.94	6.91
13	flaky	broken	36	12739.04	4550.35	0.580	-	-	-	-	-	-	-	-
14	elongated	unbroken	107	37839.32	8321.05	0.655	89	31316.50	6355.09	0.756	16.82	17.24	1.88	13.14
15	flaky	broken	55	19623.54	5133.40	0.685	-	-	-	-	-	-	-	-
26	cubic	unbroken	80	27990.60	5649.72	0.789	73	25633.70	4962.24	0.847	8.75	8.42	0.76	6.00
47	flaky	broken	45	15716.10	5393.46	0.563	-	-	-	-	-	-	-	-
48	cubic	broken	90	31865.52	7305.84	0.665	-	-	-	-	-	-	-	-
50	flaky	broken	77	27074.40	7335.95	0.594	-	-	-	-	-	-	-	-
51	flaky	broken	79	27910.41	7701.22	0.578	-	-	-	-	-	-	-	-
53	elongated	unbroken	98	35236.68	7221.27	0.720	87	30767.91	5853.42	0.811	11.22	12.68	1.25	14.79
Particle size: 50~60 mm														
Marked number	Shape	Condition after test	Initial weight (g)	Initial volume (mm ³)	Initial surface area (mm ²)	Initial 3D True Sphericity	Weight after test (g)	Volume after test (mm ³)	surface area after test (mm ²)	3D True Sphericity after test	SLAM (%)	SLAV (%)	AAD (mm)	MAD (mm)

3	elongated	unbroken	200	69971.16	11285.79	0.728	179	62764.29	9496.89	0.804	10.50	10.30	1.25	10.77
5	elongated	broken	192	67405.30	11864.53	0.675	-	-	-	-	-	-	-	-
7	cubic	unbroken	143	49907.64	9073.55	0.722	133	46506.57	8040.24	0.778	6.99	6.81	0.59	6.64
8	flaky	broken	166	58522.91	10654.38	0.684	-	-	-	-	-	-	-	-
10	cubic	broken	195	67959.02	10711.46	0.752	-	-	-	-	-	-	-	-
11	flaky	broken	88	30733.13	7572.80	0.627	-	-	-	-	-	-	-	-
13	elongated	unbroken	166	58711.16	9951.62	0.734	154	54154.11	8692.18	0.796	7.23	7.76	0.73	6.53
25	elongated	broken	214	75179.01	12866.36	0.670	-	-	-	-	-	-	-	-
29	flaky	broken	96	33616.68	9015.33	0.559	-	-	-	-	-	-	-	-
30	flaky	broken	97	33827.11	7764.89	0.651	-	-	-	-	-	-	-	-
33	cubic	unbroken	166	58431.71	9202.25	0.791	155	54039.37	8050.58	0.859	6.63	7.52	0.79	4.74
34	cubic	broken	163	57554.06	8635.02	0.835	-	-	-	-	-	-	-	-
35	flaky	broken	69	24448.11	6311.03	0.645	-	-	-	-	-	-	-	-

Table A.2 LAA loss of three groups: the flaky or elongated, cubic and scanned LAA loss

Design variance	50~60 mm			40~50 mm			25~35 mm		
	Initial weight (kg)	Weight after test (kg)	LAA loss (%)	Initial weight (kg)	Weight after test (kg)	LAA loss (%)	Initial weight (kg)	Weight after test (kg)	LAA loss (%)
Scanned	1.955	1.671	14.53	1.319	1.074	18.57	0.834	0.731	12.35
Flaky or elongated	2.066	1.754	15.10	3.102	2.504	19.28	2.467	2.068	16.17
Cubic	0.988	0.947	4.15	0.559	0.529	5.37	1.705	1.506	11.67
Tiny fragment	-	0.024	-	-	0.107	-	-	0.139	-
total	5.009	4.396	12.24	4.98	4.214	15.38	5.006	4.444	11.23